Earth Planets Space, **64**, 1231–1238, 2012

Strain anomalies induced by the 2011 Tohoku Earthquake (M_w 9.0) as observed by a dense GPS network in northeastern Japan

Mako Ohzono[1], Yasuo Yabe[2], Takeshi Iinuma[2,3], Yusaku Ohta[2], Satoshi Miura[4], Kenji Tachibana[2], Toshiya Sato[2], and Tomotsugu Demachi[2]

[1]*Institute of Seismology and Volcanology, Graduate School of Science, Hokkaido University, Sapporo 060-0810, Japan*
[2]*Research Center for Prediction of Earthquakes and Volcanic Eruptions, Graduate School of Science, Tohoku University, Sendai 980-8578, Japan*
[3]*International Research Institute of Disaster Science, Tohoku University, Sendai 980-8578, Japan*
[4]*Earthquake Research Institute, the University of Tokyo, Tokyo 113-0032, Japan*

(Received December 26, 2011; Revised May 7, 2012; Accepted May 24, 2012; Online published January 28, 2013)

We have evaluated an anomalous crustal strain in the Tohoku region, northeastern Japan associated with a step-like stress change induced by the 2011 off the Pacific coast of Tohoku Earthquake (M_w 9.0). Because the source area of the event was extremely large, the gradient of the observed eastward coseismic displacements that accompanied uniform stress change had a relatively uniform EW extension in northeastern Japan. Accordingly, the deformation anomaly, which is determined by subtracting the predicted displacement in a half-space elastic media from the observed displacement, should reflect the inhomogeneity of the rheology, or stiffness, of the crust. The difference of the EW extension anomaly between the forearc and backarc regions possibly indicates a dissimilarity of stiffness, depending on the crustal structure of the Tohoku region. The Ou-backbone range—a strain concentration zone in the interseismic period—shows an extension deficit compared with predictions. A low viscosity in the lower crust probably induced a relatively small extension. Meanwhile, the northern part of the Niigata-Kobe tectonic zone, another strain concentration zone, indicates an excess of extensional field. This is probably caused by a low elastic moduli of the thick sedimentation layer. The detection of strain anomalies in the coseismic period enables a new interpretation of the deformation process at strain concentration zones.
Key words: Coseismic strain anomaly, 2011 Tohoku Earthquake, structural heterogeneity, strain concentration zone.

1. Introduction

Plate convergence between the Pacific and Okhotsk (or North American) plates has led to the formation of an EW compressional stress field that constrains the tectonic activity of the Tohoku region in northeastern Japan (Fig. 1). Contemporary global positioning system (GPS) measurements have revealed a strain concentration zone along the Ou-backbone range (OBR), which runs through the center of the Tohoku region (Miura *et al*., 2004; Fig. 1). Previous research has shown that this strain concentration zone is caused by a weakening of the lower crust, or upper mantle, because of the existence of aqueous fluids transported through a subduction-induced upwelling fluid-flow in the mantle wedge (Hasegawa *et al*., 2005). Indeed, a number of damaging earthquakes have occurred along the OBR in the Tohoku region, such as the Riku-u earthquake (M 7.2) in 1896 and the Iwate-Miyagi inland earthquake (M 7.2) in 2008 (Fig. 1). The existence of a weakened viscoelastic layer in the lower crust beneath the OBR is also recognized by a study of rock mechanics and geological strain rate (Muto, 2011), and viscoelastic relaxation from GPS measurements after the 2008 Iwate-Miyagi inland earthquake (Ohzono *et al*., 2012). Thus, we hypothesize that stresses have relaxed considerably as inelastic deformations in the lower crust and have been transferred to the upper crust, resulting in a large strain accumulation rate there. It is further hypothesized that to release this accumulated strain, reverse faults are activated along the eastern and western edge of the OBR.

As recorded by a nationwide continuous global navigation satellite system (GNSS) network, GEONET, and seafloor geodetic observations, unprecedented large coseismic surface displacements around the Tohoku region were generated by the 2011 off the Pacific coast of Tohoku Earthquake (hereinafter, the Tohoku earthquake, M_w 9.0), Japan (e.g., Ozawa *et al*., 2011; Sato *et al*., 2011). The step-like coseismic deformation caused by the earthquake released the accumulated elastic strain to generate an EW extension over the region. Here, if there is a uniform elastic crust under the Tohoku region, the difference between the predicted strain distribution, estimated from a half-space elastic fault model such as that of Okada (1992), and the observed strain distribution, will become zero. However, assuming that the lower crust beneath the strain concentration zone has already relaxed to some extent, as suggested in the hypothesis, the elastic strain accumulation over the crust thickness is smaller than that of the surrounding area. Therefore, the

doi:10.5047/eps.2012.05.015

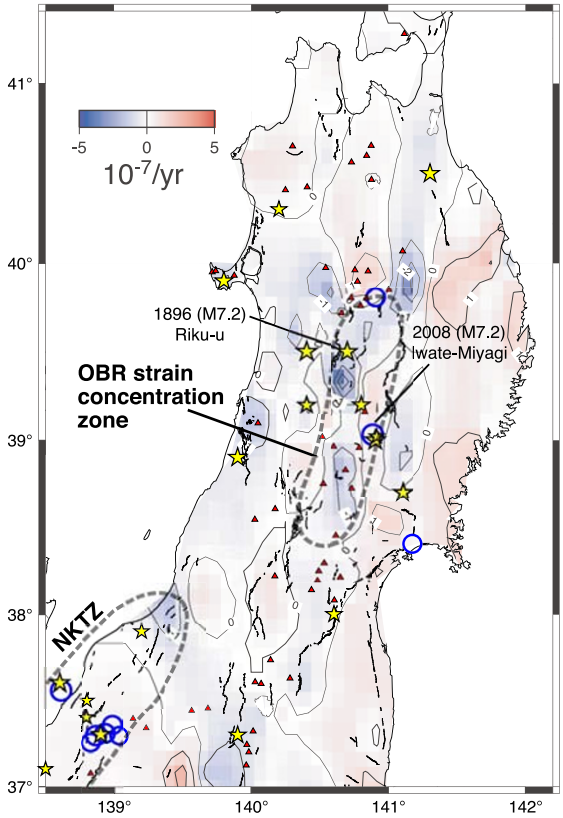

Fig. 1. EW strain rate calculated from the GPS velocity field for the period from 1997 to 2001 (after figure 6(b) in Miura *et al*., 2004). The effect of interplate coupling is eliminated from a predicted model (Suwa *et al*., 2006). Blue and red areas denote contraction and extension, respectively. The effect of interplate coupling is eliminated. Solid lines represent traces of the inland active fault (Nakata and Imaizumi, 2002). Red triangles indicate Quaternary active volcanoes. Gray dashed lines encircle strain concentration zones of the Ou-backbone Range (OBR) and the northeastern part of the Niigata-Kobe Tectonic Zone (NKTZ). Stars represent the epicenters of damaging earthquakes since 1896. Blue circles represent the epicenters of inland earthquakes (larger than M_w 6) from October 1997 to March 10, 2011.

coseismic EW extension of the upper crust overlaying a relaxed lower crust in the OBR should be smaller than that in other regions. The image of this hypothesis is shown in Fig. 2(a).

On the other hand, there is also the possibility that the strain concentration zone during the interseismic period is an indication of a small stiffness of the crust. The low seismic velocity beneath the OBR (Nakajima *et al*., 2001) suggests low elastic moduli there. It is also known that the northern part of the Niigata-Kobe Tectonic Zone (NKTZ) is covered by a thick sediment having a low seismic velocity (Kato *et al*., 2009). A region with smaller stiffness has the potential to accumulate a larger elastic strain during the interseismic period. The large elastic strain should then be released when a megathrust event occurs along the subducting plate boundary off the Pacific coast of Tohoku. These images are shown in Figs. 2(b) and 2(c).

It is difficult to distinguish the two possibilities for the origin of the strain concentration zone (inelastic relaxation of the lower crust, or a compliant elastic crust) from interseismic deformation, because both causes show a similar response to the interseismic slow loading. However, their behaviors against such quick unloading as associated with the Tohoku earthquake are opposite each other. Accordingly, coseismic EW extension anomalies can serve as a good measure to test the hypothesis of a strain concentration zone along the OBR and the northern part of the NKTZ. The coseismic deformation field induced by the Tohoku earthquake has been evaluated using the dense regional GPS network operated by Tohoku University in combination with GEONET.

2. Data and Method

Continuous GPS sites complementing the GEONET configuration were established to comprehensively monitor (a) the crustal deformation caused by the subduction of the Pacific plate, (b) the activity of volcanoes, and (c) the loading of inland active faults in the Tohoku region.

The GPS sites used in the present study are plotted in Fig. 3. In order to understand the coseismic displacement, we estimate the daily site coordinates before (10 March, 2011) and after (11 March, 2011) the mainshock, using Bernese GPS Software version 5.0 (Dach *et al*., 2007). The coseismic displacements at each site are calculated from the coordinate differences before, and after, the mainshock. In the analyses, we use the precise ephemerides and Earth rotation parameters made available by the International GNSS Service (IGS). The coordinates are based on the International Terrestrial Reference Frame 2008 (Altamimi *et al*., 2011) and determined by constraining the daily coordinates of four IGS sites around Japan (AIRA, DAEJ, KHAI, and YSSK). On the day of the mainshock (11 March, 2011), we adopt the time period of the RINEX data after the origin time (5:47 GPS time) to avoid contamination of the displacement before this event. Therefore, the coordinates on the day of the mainshock are determined solely from the carrier-phase data for approximately 18 hours after the earthquake. The horizontal displacement vectors at each site relative to the GEONET site, 1093 (Fig. 3), are shown with black arrows in Fig. 4(a).

The coseismic displacement field is reproduced by a simple fault model, so as to avoid a trade-off between the complexities of crustal structure and heterogeneous slip distribution during the modeling. The inversion method of Matsu'ura and Hasegawa (1987) is adopted, under the assumption of a uniform slip on two rectangular faults that are located on the plate boundary, in a homogeneous elastic half-space. *A priori* fault parameters are assumed, based on a model proposed by the Geospatial Information Authority of Japan (GSI, http://www.gsi.go.jp/cais/topic110422-index.html); the resulting fault parameters are listed in Table 1. A comparison of the observed and calculated horizontal displacements is shown in Fig. 4(a). The strain calculation from the displacement data is based on the method developed by Shen *et al*. (1996) and Sagiya *et al*. (2000). As an example, the observed dilatation strain and the principal strain axis are plotted in Fig. 4(b).

To extract the strain anomaly caused by inhomogeneity of the subsurface structure, a strain change residual (SC-residual, the difference between the observed and calculated EW strain) is calculated using the observed and calculated coseismic strain field. The resultant EW component

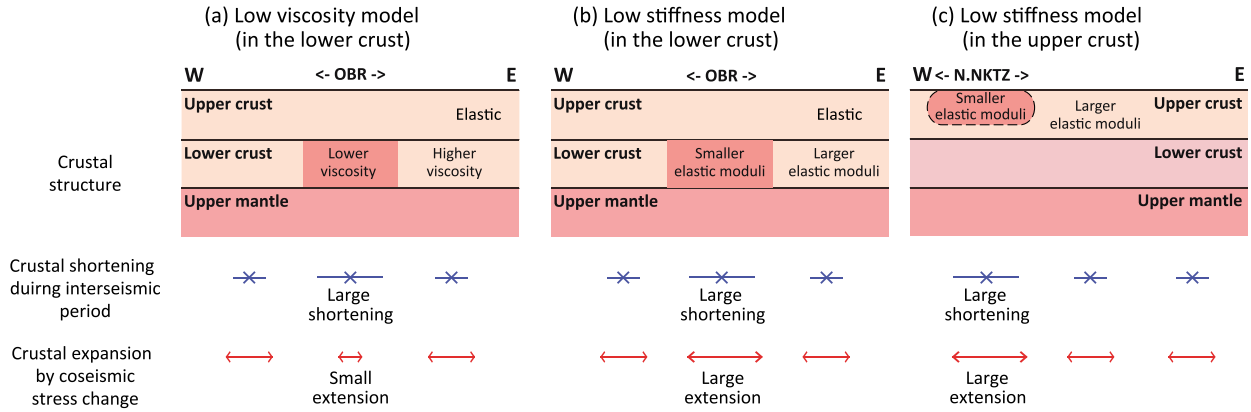

Fig. 2. Schematic images of surface strain, which depends on the crustal structure, around the two strain concentration zones, the OBR and the northern part of the NKTZ in the Tohoku region. The assumed crustal structure and their surface strain pattern during the interseismic period and the coseismic period are shown. (a) Low viscosity model in the lower crust. The viscosity in the lower crust beneath the OBR is assumed to be lower than in the other fields. (b) Low elastic modulus model in the lower crust. The elastic modulus in the lower crust beneath the OBR is assumed to be lower than in the other fields. (c) Low elastic modulus model in the upper crust. The elastic modulus in the upper crust beneath the NKTZ is assumed to be lower than in the other fields due to the existence of thick sediments.

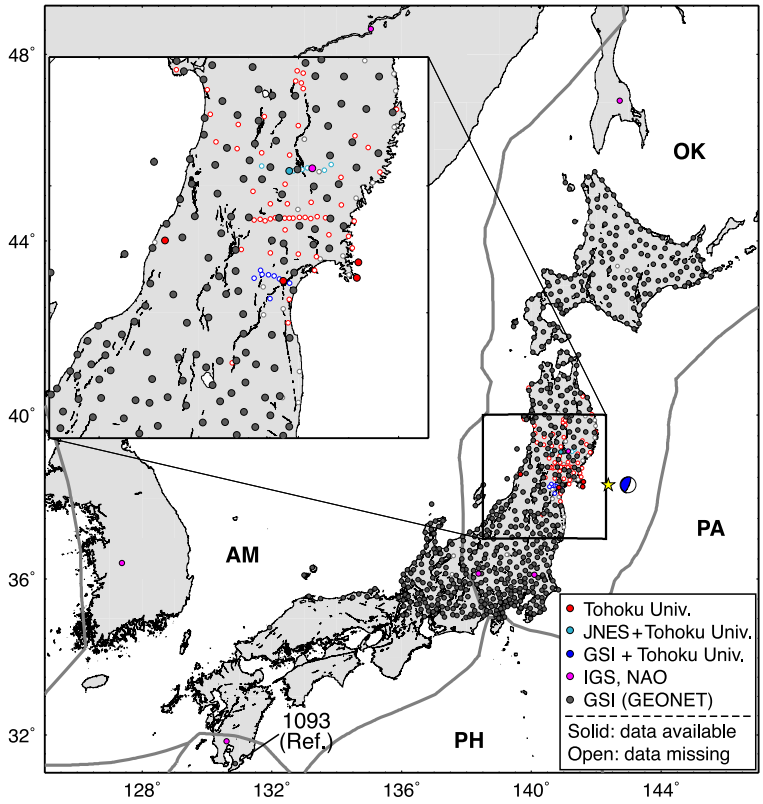

Fig. 3. Distribution of continuous GPS sites. Each symbol denotes an installed institution or laboratory (red: Tohoku University; light blue: collaboration of JNES and Tohoku university; blue: collaboration of GSI and Tohoku university; pink: IGS (MIZU), and NAO; gray: GSI (GEONET)). Coseismic displacements were obtained at the colored sites at the sites indicated by solid circles.

of the SC-residual is shown in Fig. 5(a). The further the distance from the source area, the smaller the coseismic stress change that is induced by an earthquake. Therefore, the amplitudes of the SC-residual along the Japan Sea coast can be smaller than those along the Pacific coast, even if both areas have the same level of rheological anomalies. To eliminate the effect of the geometrical spreading, the ratios of the observed coseismic strain changes to the calculated ones (SC-ratio) at each grid (every 0.01° in the present study) are also shown in Fig. 5(b).

In the present study, the distance decay constant (DDC), which controls the weighting of the observations, is assumed to be 20 km. In the strain calculation, GPS sites located in an area of 2 × DDC from a grid become the subject of weighting (formula (3) in Sagiya *et al.*, 2000). The GPS sites are located every ∼20 km, on average. Therefore, it is desirable to assume a DDC over ∼15 km to include plural sites. The number of included sites in the calculation at each grid is plotted in Fig. 5(c). On the other hand, because the strain concentration zone along the OBR has a width of

Table 1. Estimated fault parameters.

Fault plane	Longitude* [deg.]	Latitude* [deg.]	Depth* [km]	Length [km]	Width [km]	Strike [deg.]	Dip [deg.]	Rake [deg.]	Slip [m]	M_w**
North	143.987	38.804	3.5	191.5	143.2	206	16	104	18.0	8.80***
South	142.789	37.344	8.6	191.9	98.7	202	15	80	5.8	8.36***

*Fault location is northern corner of the upper edge.
**Rigidity is assumed to be 40 GPa.
***Total moment magnitude is 8.86.

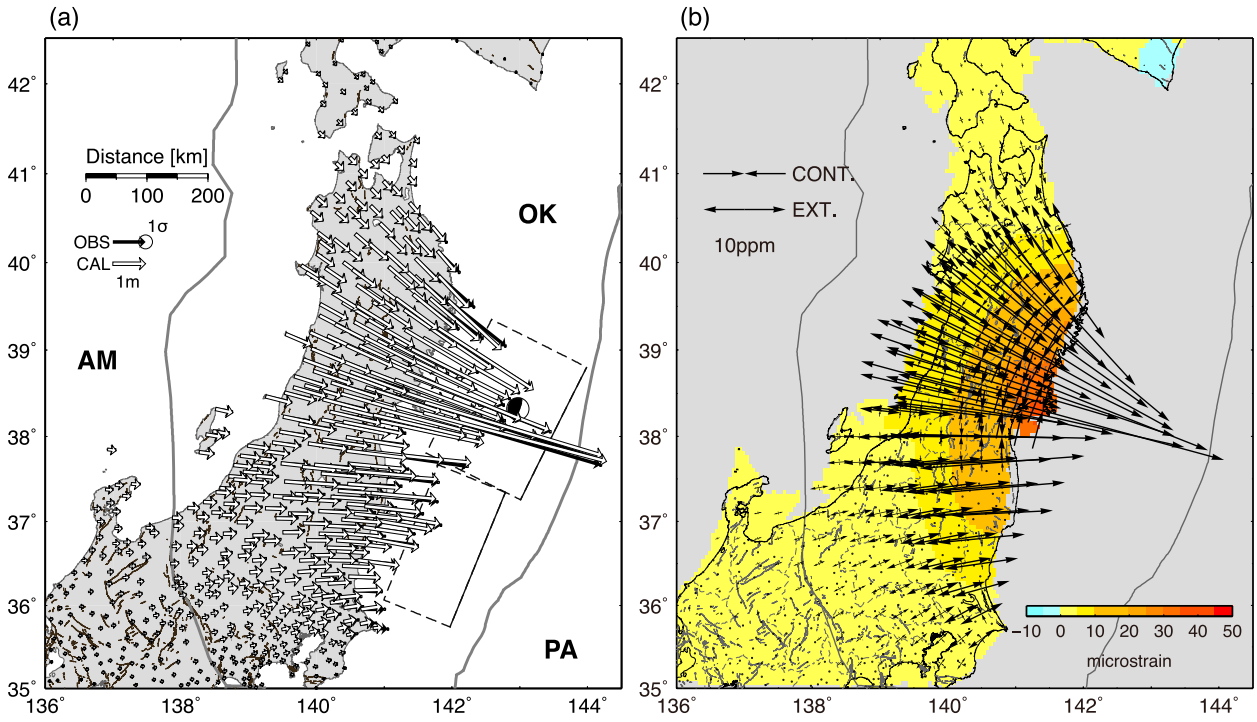

Fig. 4. (a) Horizontal displacement induced by the 2011 Tohoku earthquake. The reference site is a GEONET site, 1093. Black and white arrows represent observed and calculated horizontal displacement vectors from the simple fault model, respectively. The two rectangles with a solid line indicating an upper fault edge represent the surface projection of the estimated fault model. The focal mechanism solution of the mainshock provided by a W-phase analysis (http://earthquake.usgs.gov/earthquakes/eqinthenews/2011/usc0001xgp/neic_c0001xgp_wmt.php) is shown at the epicenter. Solid gray lines indicate plate boundaries after Bird (2003). PA, OK, and AM are abbreviations for the Pacific, Okhotsk, and Amurian plates, respectively. (b) Dilatation strain (color, positive value means expansion) and principal strain axis (vectors) calculated from coseismic displacement.

$<\sim$40 km, a smaller DDC should be applied to recognize such a local strain field. Thus, we also considered the case of DDC $=$ 15 km (Figs. 5(d), 5(e), and 5(f)). The result indicates a detailed strain anomaly distribution. However, because several areas have only a few sites for the calculation, we use the results of DDC $=$ 20 km here.

3. Results and Discussion

The distributions of the SC-residual and SC-ratio in the EW component are shown in Figs. 5(a) and 5(b), respectively. In this study, we focused on the region between 37°N and 40°N, which experienced significant displacement during the Tohoku earthquake. In Figs. 5(a) and 5(b), blue and red areas indicate the places where the observed strain change is smaller (extension deficit, ED) and larger (extension excess, EE) than the calculation, respectively. However, these values change depending on the assumed elastic moduli in the fault modeling. To see the relative spatial pattern SC-ratio around the OBR, we also show profiles between 139.5°E and 141.5°E crossing 38.0°N, 38.3°N, 38.6°N, 38.9°N, 39.2°N, and 39.5°N in Fig. 6.

3.1 General pattern in Tohoku region

In Figs. 5(a) and 5(b), it seems that the ED area is distributed along the Pacific coast and EE area along the Japan Sea coast. This pattern may raise the possibility of a difference in the deformability of the forearc (eastern part) and backarc (western part) of the crust. In the interseismic period, the strain rate field indicates a tendency for a relatively small contraction in the forearc region and a large contraction in the backarc region (Miura *et al.*, 2004; Fig. 1). These are common features in both the coseismic and interseismic periods (small deformation in the forearc region and large deformation in the backarc region). In addition, seismic tomography also indicates a high-velocity field in the forearc region and a low-velocity field in the backarc region at the depth of 10 km (Nakajima *et al.*, 2001). This ED and EE distribution pattern possibly indicates a regional-scale difference in the stiffness of the crust (forearc $>$ backarc) over the Tohoku region.

3.2 Strain anomaly along the OBR

In Fig. 6, it is clear that a smaller SC-ratio is distributed along the OBR strain concentration zone more than that of

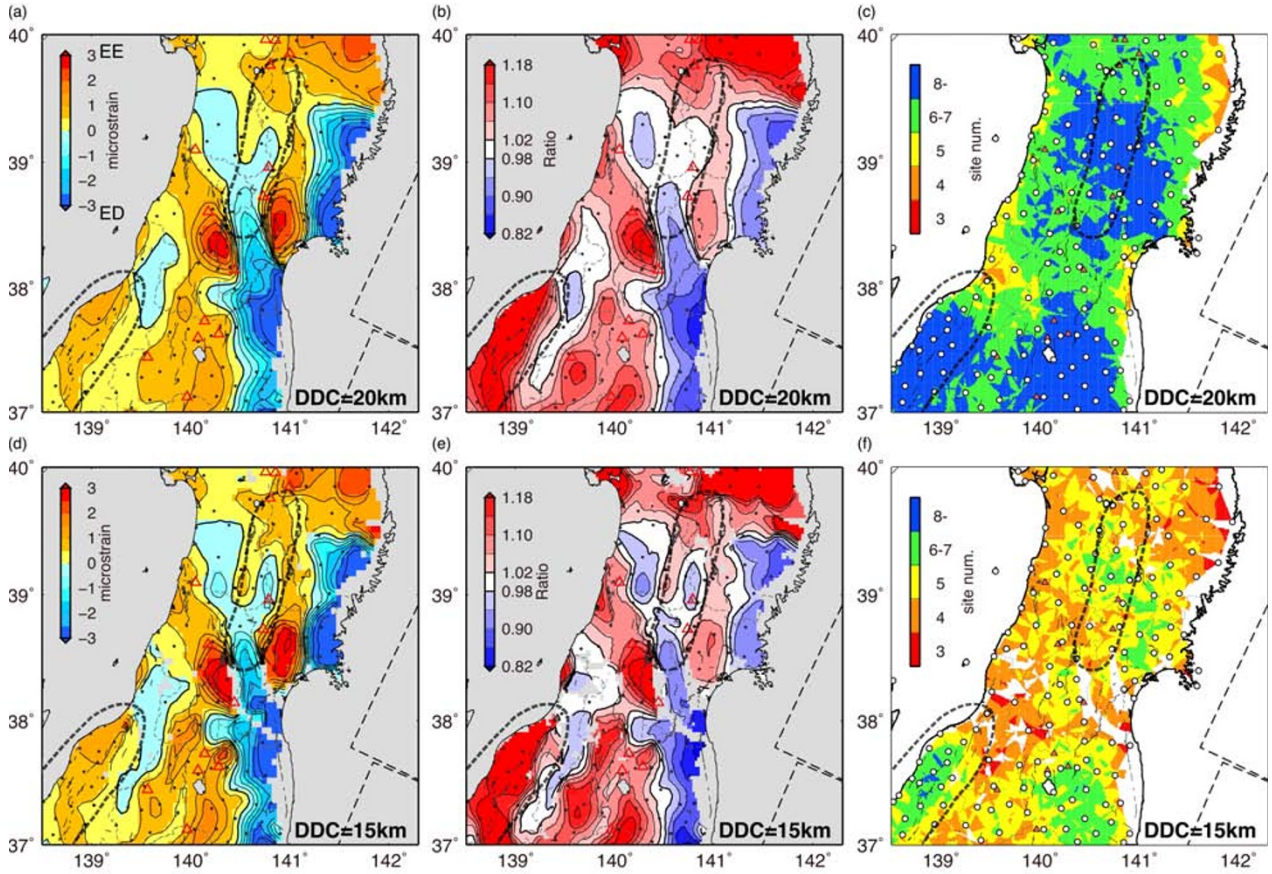

Fig. 5. (a) Distribution of the EW component of the strain change residual (observation−calculation) calculated at each site. Blue and red areas denote the extension deficit (ED; observation is smaller than calculation) and the extension excess (EE; observation is larger than calculation), respectively. Gray dashed lines encircle the same strain concentration zones as shown in Fig. 1. Open triangles are Quaternary active volcanoes. The thick and thin contour lines indicate 0 and every 0.5×10^{-6} strain, respectively. Dots are GPS site locations. (b) Same as (a) but with the distribution of the ratios of strain change in the EW component (observation/calculation). The thick and thin contour lines indicate 1 and every 0.02, respectively. (c) The number of included sites for the weighting in the strain calculation at each grid (every 0.01°). The color is filled when the number of included sites is larger then three. (d), (e) and (f) Same as (a), (b), and (c) but the distance decay constant (DDC) is 15 km instead of 20 km.

the surrounding region. The observed crustal deformation (EW extension) in a part of the strain concentration zone along the OBR was up to 15% smaller than fault model predictions, which assume a uniform slip in an isotropic homogeneous elastic media. Consistent with the hypothesis of Hasegawa *et al.* (2005), who suggested a relaxation in the lower crust beneath the strain concentration zone, a blue area exists in both figures along the OBR between 38°N and 39.3°N, indicating that this region has relaxed more. This idea is shown in Fig. 2(a). In the smaller scale in the case of DDC = 15 km, although this does not give a good spatial coverage, we also confirm a clear ED region along the OBR strain concentration zone. This can be attributed to the condition of the crustal structure beneath the OBR.

In this OBR strain concentration zone, there is a variation of the strain distribution (Figs. 5 and 6) along north to south. The SC-ratio becomes larger going north. The area to the north of 39.0°N is located between two reverse active faults (the Kitakami-teichi-seien fault and the Yokote-bouchi-toen fault) with less active volcanoes. Therefore, this may imply a higher viscosity due to low temperature in its lower crust than that of the south ED region. A large strain concentration during the interseismic period, and a larger extension associated with the Tohoku earthquake, indicates a small stiffness of the crust in this area. Because this area is not a sedimentation region, a small stiffness is not the case for the upper crust. A large EW extension is possibly the result of a low elastic modulus in the lower crust. This corresponds to Fig. 2(b). However, in this strain concentration zone, the number of GPS sites in the north area is less than that of south area (Fig. 5(c)). Therefore, there is another possibility that the effect outside the strain concentration zone could be contaminated in the northern part.

3.3 Other characteristic region

Several characteristic areas are shown in Fig. 5. The most interesting area is the northern part of the NKTZ. This is another well-known strain concentration zone in central Japan (Fig. 1, Sagiya *et al.*, 2000). The EE region is a result of a response of the northeastern part of the NKTZ to a step-like stress perturbation. Although both the OBR and the northeastern part of the NKTZ behave as a strain concentration zone under long-term slow loading, they responded differently to step-like stress changes induced by the Tohoku earthquake. The northern part of the NKTZ (Niigata basin) is formed by Miocene sedimentation. Therefore, its elastic modulus is thought to be smaller than other regions. The seismic velocity structure shows that the surface layer of small P-wave velocity (<5 km/s) extends to 10 km in depth

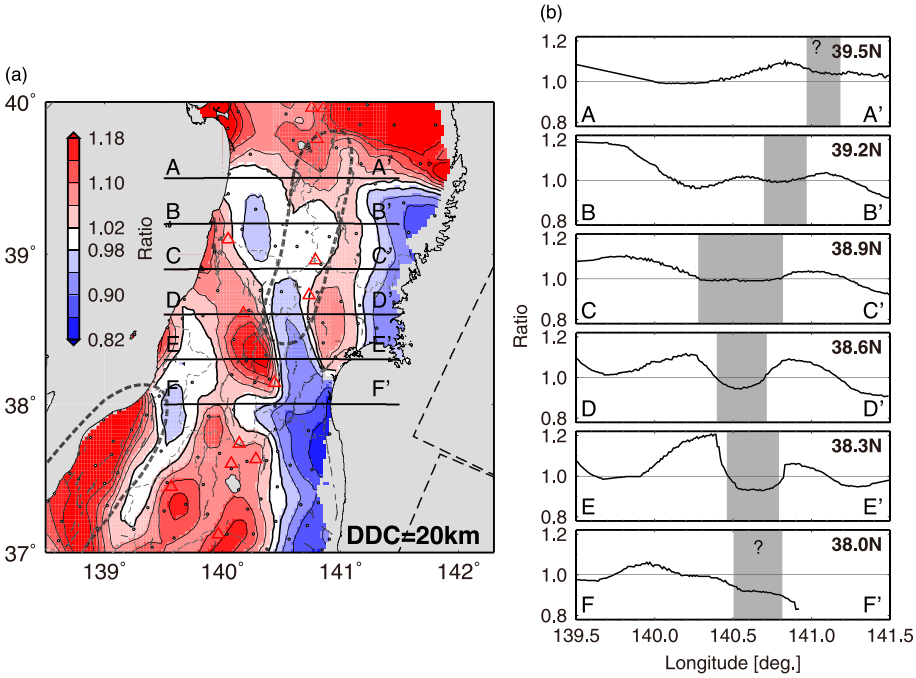

Fig. 6. SC-ratio profiles. (a) Same as Fig. 5(b). Six lines crossing east to west are the profile line of (b). (b) SC-ratio profile between 139.5°E and 141.5°E crossing 39.5°N (A–A′), 39.2°N (B–B′), 38.9°N (C–C′), 38.6°N (D–D′), 38.3°N (E–E′), and 38.0°N (F–F′). Shadow areas correspond to the OBR strain concentration zone.

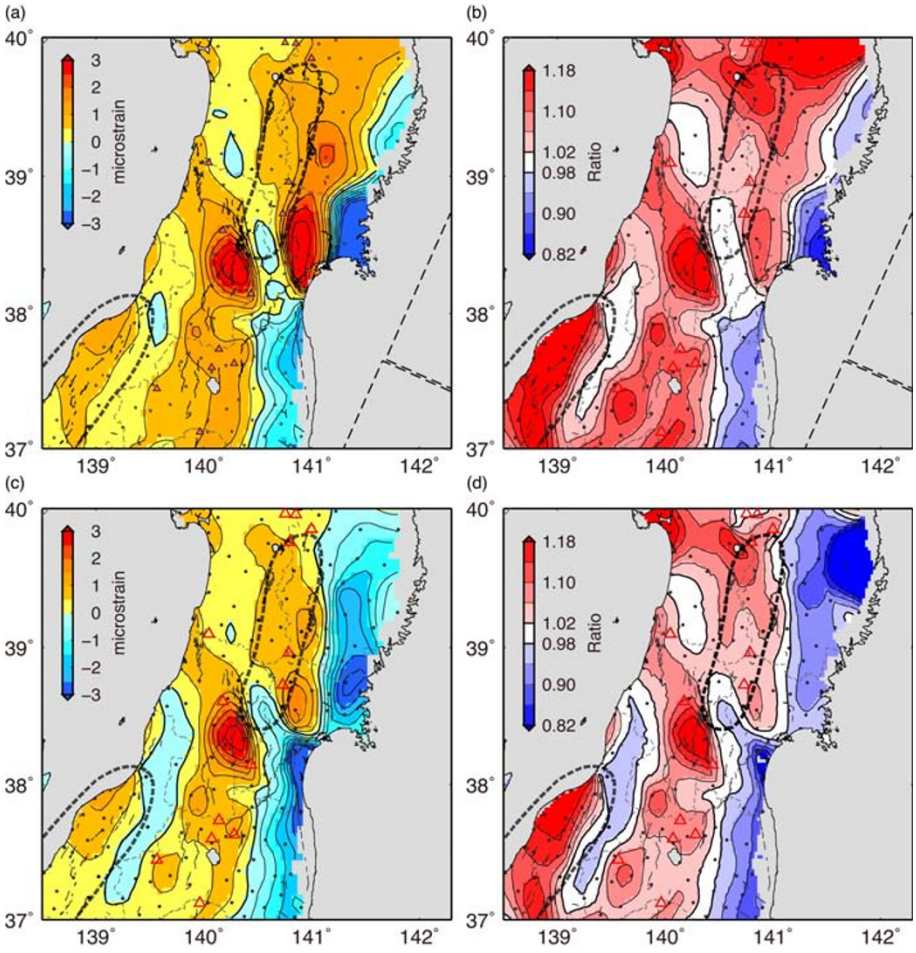

Fig. 7. (a) and (b) same as Fig. 5(a) and Fig. 5(d), respectively, but the estimation is obtained from a fault model based on Nishimura *et al*. (2011). (c) and (d) same as Fig. 5(a) and Fig. 5(d), respectively, but the estimation is obtained from the fault model of Iinuma *et al*. (2011), under the assumption of an inhomogeneous coseismic slip distribution.

(Kato *et al.*, 2009). A detailed discussion necessitates an examination of the deformation processes in the respective regions using numerical modeling, such as a finite element method that considers an inhomogeneous structure. The evidence suggests that the OBR and northeastern part of the NKTZ strain concentration zones may have been formed under a different crustal rheology.

The EE regions also appear at the eastern and western side of the ED region in the OBR. The former is considered to be a branch of the strain concentration zone along the OBR (Miura *et al.*, 2004). These areas correspond to sedimentary basins (Sendai and Yamagata basins). The same mechanism as in the case of the NKTZ can be applied to the eastern branch of the strain concentration zone. A small stiffness in the upper crust is expected (Fig. 2(c)).

3.4 Dependency of coseismic fault model

To emphasize the strain anomaly caused by the inhomogeneous crustal structure, a simple source model consisting of two rectangular faults with a uniform slip was adopted. It is possible that strain heterogeneity, caused by a larger number of rectangular faults and/or a heterogeneous slip distribution, was misinterpreted as being anomalies relating to an inhomogeneous crustal structure. To confirm this, we calculated the SC-residual and SC-ratio using two slip models. One is a rectangular fault model with a uniform slip based on Nishimura *et al.* (2011), which consists of five rectangular faults, including two large aftershocks which occurred immediately after the mainshock. The calculated SC-residual and SC-ratio is shown in Figs. 7(a) and 7(b), respectively. Comparing Fig. 5(a) with Fig. 7(a), the ED and EE distribution patterns are mostly consistent with each other. Therefore, two models of a uniform rectangular fault slip in an elastic media explain the observed crust deformation in the strain concentration zone in a same manner. However, the value and extent of the ED region at the east coast becomes small when the five rectangular faults are applied. It is possible that there is some effect of fault geometry in this area, due to the proximity of faults.

Another fault model is a non-uniform coseismic slip model estimated by Iinuma *et al.* (2011) (Figs. 7(c) and 7(d)). The SC-residual and SC-ratio indicates the existence of an ED region in the forearc and an EE region in the backarc. Therefore, the regional-scale variation in stiffness is also reflected in the same way as the result of simple rectangular fault model cases. The SC-ratio in the OBR strain concentration zone (Fig. 7(d)) shows a low value compared with the surrounding region. The variation of this strain anomaly pattern is not affected by the different fault models.

4. Conclusion

We have examined the crustal response, in the Tohoku region, to a step-like stress change induced by the 2011 Tohoku earthquake. The observed crustal deformation (EW extension) in a part of the strain concentration zone along the OBR was up to 15% smaller than predictions based on a source model, which assumes a uniform slip on two rectangular faults, in an isotropic homogeneous elastic media. In the Tohoku region, the ED area is distributed in the forearc region, while the EE area is distributed in the backarc region. This distribution pattern possibly indicates a regional variation in stiffness according to the crustal structure. The response of a southern part of the strain concentration zone along the OBR to an instantaneous unloading caused by the earthquake was consistent with that expected of a region for a model in which stresses in the lower crust and/or the uppermost mantle have been inelastically relaxed under a long-term slow loading (Hasegawa *et al.*, 2005). On the other hand, the EE region in the northern part of the OBR possibly reflects a low elastic stiffness in the lower crust rather than a flow in the lower crust. In addition, although both the northeastern part of the NKTZ and the OBR behave as the strain concentration zones under a long-term slow loading, their responses to instantaneous unloading look different. This finding suggests that the crust and/or uppermost mantle of the northeastern part of the NKTZ and the OBR have different rheological characteristics. In conclusion, strain concentration zones exhibit a variety of responses against step-like unloading. This evidence represents a new constraint to the rheology model of the crust and uppermost mantle beneath northeast Japan.

Acknowledgments. The GPS data were obtained from a research project conducted by the Japanese Nuclear Energy Safety Organization to establish evaluation techniques for seismogenic faults, the Geospatial Information Authority of Japan, and the Mizusawa VLBI Observatory of the National Astronomical Observatory of Japan. We thank Dr. J. Muto for the discussion of rheological structure in the Tohoku region. We are grateful to two anonymous reviewers and an editor, Prof. Dr. A. Hasegawa, for useful discussions and comments to improve this paper. Most of the figures were generated using the GMT software (Wessel and Smith, 1998).

References

Altamimi, Z., X. Collilieux, and L. Mtivier, ITRF2008: An improved solution of the international terrestrial reference frame, *J. Geod.*, **85**, 457–473, doi:10.1007/s00190-011-0444-4, 2011.

Bird, P., An updated digital model of plate boundaries, *Geochem. Geophys. Geosyst.*, **4**, 1027, doi:10.1029/2001GC000252, 2003.

Dach, R., U. Hugentobler, P. Fridez, and M. Meindl, *Bernese GPS Software Version 5.0 User Manual*, 612 pp., Astronomical Institute, University of Bern, Bern, 2007.

Hasegawa, A., J. Nakajima, N. Umino, and S. Miura, Deep structure of the northeastern Japan arc and its implications for crustal deformation and shallow seismic activity, *Tectonophysics*, **403**(1–4), 59–75, doi:10.1016/j.tecto.2005.03.018, 2005.

Iinuma, T., M. Ohzono, Y. Ohta, and S. Miura, Coseismic slip distribution of the 2011 off the Pacific coast of Tohoku Earthquake (*M* 9.0) estimated based on GPS data—Was the asperity in Miyagi-oki ruptured?, *Earth Planets Space*, **63**, 643–648, doi:10.5047/eps.2011.06.013, 2011.

Kato, A., E. Kurashimo, T. Igarashi, S. Sakai, T. Iidaka, M. Shinohara, T. Kanazawa, T. Yamada, N. Hirata, and T. Iwasaki, Reactivation of ancient rift systems triggers devastating intraplate earthquakes, *Geophys. Res. Lett.*, **36**, L05301, doi:10.1029/2008GL036450, 2009.

Matsu'ura, M. and Y. Hasegawa, A maximum likelihood approach to nonlinear inversion under constraints, *Phys. Earth Planet. Inter.*, **47**, 179–187, 1987.

Miura, S., T. Sato, A. Hasegawa, Y. Suwa, K. Tachibana, and S. Yui, Strain concentration zone along the volcanic front derived by GPS observations in NE Japan arc, *Earth Planets Space*, **56**, 1347–1355, 2004.

Muto, J., Rheological structure of northeastern Japan lithosphere based on geophysical observations and rock mechanics, *Tectonophysics*, **503**, 201–206, doi:10.1016/j.tecto.2011.03.002, 2011.

Nakajima, J., T. Matsuzawa, A. Hasegawa, and D. Zhao, Three-dimensional structure of Vp, Vs, and Vp/Vs beneath northeastern Japan: Implications for arc magmatism and fluids, *J. Geophys. Res.*, **106**, 21843–21857, 2001.

Nakata, T. and T. Imaizumi (eds.), *Digital Active Fault Map of Japan* (with

2 DVDs), University of Tokyo Press, Tokyo, 2002 (in Japanese).

Nishimura, T., H. Munekane, and H. Yarai, The 2011 off the Pacific coast of Tohoku Earthquake and its aftershocks observed by GEONET, *Earth Planets Space*, **63**, 631–636, doi:10.5047/eps.2011.06.025, 2011.

Ohzono, M., Y. Ohta, T. Iinuma, S. Miura, and J. Muto, Geodetic evidence of viscoelastic relaxation after the 2008 Iwate-Miyagi Nairiku earthquake, *Earth Planets Space*, **64**, 759–764, doi:10.5047/eps.2012.04.001, 2012.

Okada, Y., Internal deformation due to shear and tensile faults in a half-space, *Bull. Seismol. Soc. Am.*, **82**, 1018–1040, 1992.

Ozawa, S., T. Nishimura, H. Suito, T. Kobayashi, M. Tobita, and T. Imakire, Coseismic and postseismic slip of the 2011 magnitude-9 Tohoku-Oki earthquake, *Nature*, **475**, 373–376, doi:10.1038/nature10227, 2011.

Sagiya, T., S. Miyazaki, and T. Tada, Continuous GPS array and present-day crustal deformation of Japan, *Pure. Appl. Geophys.*, **157**, 2303–2322, 2000.

Sato, M., T. Ishikawa, N. Ujihara, S. Yoshida, M. Fujita, M. Mochizuki, and A. Asada, Displacement above the hypocenter of the 2011 Tohoku-Oki Earthquake, *Science*, doi:10.1126/science.1207401, 2011.

Shen, Z.-K., D. D. Jackson, and B. X. Ge, Crustal deformation across and beyond the Los Angeles basin from geodetic measurements, *J. Geophys. Res.*, **101**, 27957–27980, doi:10.1029/96JB02544, 1996.

Suwa, Y., S. Miura, A. Hasegawa, T. Sato, and K. Tachibana, Interplate coupling beneath NE Japan inferred from three-dimensional displacement field, *J. Geophys. Res.*, **111**, B04402, doi:10.1029/2004JB003203, 2006.

Wessel, P. and W. H. Smith, New, improved version of the Generic Mapping Tools released, *Eos Trans. AGU*, **79**, 579, 1998.

M. Ohzono (e-mail: m.ohzono@mail.sci.hokudai.ac.jp), Y. Yabe, T. Iinuma, Y. Ohta, S. Miura, K. Tachibana, T. Sato, and T. Demachi